THE OHIO STATE UNIVERSITY

Levy Walks and Turbulent Flows

Fernand Hayot
Department of Physics

Office of the Chief of Naval Research
Arlington, VA 22217-5000

Grant No. N00014-92-J-1271
1994 Annual Report

January 1995

THE OHIO STATE UNIVERSITY

Levy Walks and Turbulent Flows

Fernand Hayot
Department of Physics

Office of the Chief of Naval Research
Arlington, VA 22217-5000

Grant No. N00014-92-J-1271
1994 Annual Report
RF Project No. 769633/725740

January 1995

"This material is based upon work supported by the Department of the Navy, Office of the Chief of Naval Research, under Grant No. N00014-92-J-1271

"Any opinions, findings, and conclusions of recommendations expressed in this publication are those of the author(s) and do not necessarily reflect the views of the Department of the Navy, Office of the Chief of Naval Research."

1994 Report on ONR Grant No. N00014-92-J-1271.

LEVY WALKS AND TURBULENT FLOWS.

Fernand Hayot

Department of Physics

The Ohio State University

I. Area of Research and Focus

The present grant started in January of 1992, and was renewed in January of 1993. It provides support for one graduate student, Luke Wagner.

The focus of the work is turbulence, and its modelling by Lévy walks in lattice gas hydrodynamics. After studying turbulent channel flow[1], we have concentrated over the last two years on flow around an infinite cylinder. The flow situations we are concerned with are those where some level of turbulence in the incident flow affects measurements of pressure and drag on the cylinder as compared to the laminar case. We are also greatly interested in how such turbulence interferes with the coherence and behavior of the vortex street which develops behind the cylinder at sufficiently large Reynolds numbers.

Lévy walks fit naturally into the framework of lattice gas hydrodynamics[1]. They are relevant to phenomena where turbulent behavior results from the

exchange of momentum over a vast range of distances, and they provide an appealing physical picture for their description. In turbulent channel flow they are akin to Prandtl's mixing length hypothesis. In turbulent flow around a cylinder they provide a mechanism for the transfer of fluid into and out of the wake into the surrounding fluid, which is believed to be responsible for observed changes in behavior of pressure and drag[2], before one reaches the drag crisis region.

II. **WORK DONE UNDER THE GRANT**(January 1993- December 1994)

Though our initial work was done with the Boolean version of lattice gas hydrodynamics, our recent work is done with the Boltzmann version, relying on the BGK (Bhatnagar, Gross, Krook) model. The reason for the change is our interest in quantitative results for pressure and drag, and fluctuations of the vortex street. The statistical fluctuations which occur in the coarse-graining procedure in the Boolean case make it impossible to obtain precise measurements of the pressure around the cylinder. The other advantage of the Boltzmann version is that one does not need consider the very large sytems one must in the Boolean case, even for Reynolds numbers as low as 100. The disadvantage of the Boltzmann approach is that one now deals with real numbers, no longer merely integers in the main part of the algorithm, and therefore the speed of execution brought about by the use of multispin coding is lost. Our codes had therefore to be rewritten in order to implement

this different algorithmic approach.

I wish to discuss three main results, which are reported in the following three references, included with this report:

- *Pressure in lattice Boltzmann simulations of flow around a cylinder*, by Lukas Wagner, to appear in *Physics of Fluids.*

- *Lattice Boltzmann simulations of laminar and turbulent flow past a cylindrical obstacle*, by Lukas Wagner and F. Hayot, to appear in the *Journal of Statistical Physics.*

- *Lévy walks and lattice gas hydrodynamics*, by F. Hayot and Lukas Wagner, to appear in a Springer Verlag book on Lévy walks.

The three results concern pressure around the cylinder, drag and the coherence of the Von Karman vortex street.

4.1. *Pressure around the cylinder.*

Some care has to be taken to measure pressure since on the lattice the cylinder is actually a polygon. Our results concern reduced pressure as a function of the angle θ around the cylinder measured from the stagnation point. We find that over part of the forward region the turbulent pressure is higher than the laminar one, but around the back region the opposite is true, the greatest difference occuring close to , but above $\theta = \pi/2$. We also find (as expected) that the difference between laminar and turbulent pressure diminishes as the "integral scale" parameter l_{max}/D diminishes. These results are in qualitative agreement with those of Bearman[2] for flat

plates, who observed that turbulence diminishes the base pressure (behind the plate), and also that, as the size of the plate increases (for a given integral scale) the difference between turbulent and laminar base pressure diminishes.

4.2. *Drag.*

Drag on the cylinder is affected by transport of momentum into and out of the wake, which is a result of the Lévy exchanges. These exchanges lead to a clear decrease in the size of the region of negative streamwise velocity component right behind the cylinder. From a particle point of view, this means that there are fewer particles which impinge onto the cylinder hitting it from the back against the principal thrust of the flow. As a result, the drag is expected to increase as l_{max}/D increases sufficiently. This is what our results show for the drag coefficient C_D as a function of l_{max}/D. As sooon as l_{max}/D exceeds a value of 2, the drag starts increasing. It saturates when the size of the exchanges becomes large enough to be insensitive to the dimension of the vortex street itself. According to a wake entrainment argument[2], turbulent drag should increase as $(l_{max}/D)^2$ relative to the laminar case, until it saturates. Our result on turbulent drag is in qualitative agreement with this.

4.3. *Coherence of Von Karman street.*

It is natural to ask to what extent entrainment into and out of the wake, caused by the presence of turbulence in the incident flow, affects the coher-

ence of the Von Karman street. As a measure of that coherence, we choose the component v of velocity perpendicular to the streamwise direction, on the axis of the cylinder. In the laminar case, this is a strong component, which at the Reynolds number we are considering varies periodically in time with a well defined frequency, which determines the value of the Strouhal number. Our results show two things: one that v_{peak},the maximum value of v, decreases rapidly as the parameter l_{max}/D increases, and becomes very small at $l_{max}/D = 3$, the value where also the drag starts deviating significantly from the laminar value. Secondly, that though the intensity diminishes considerably, the frequency spectrum of v continues to be dominated by the Strouhal frequency component. There thus may be no significant broadening of the Strouhal peak in the spectrum as the range of exchanges increases. We have noticed however that a contour plot of pressure, which in the laminar case shows clearly the presence of vortices, changes completely as l_{max}/D becomes large enough, without any trace left of vortex structure. Correlations between transverse velocity components on and off the axis show the same phenomenon. Speaking loosely, one might say that as the range of exchanges increases the Von Karman street gradually loses its spatial coherence, but in such a way that the rate of production of vortices (the Strouhal number) remains well defined, at least up to $l_{max}/D = 2$. For clearly higher values the vortices cease to exist.

There is a caveat here: these results depend sensitively on the precise

relationship between number of exchanges and distance of exchange in the Lévy walks, whereas those on pressure for instance do not. It is therefore worth repeating here that as far as the coherence of the Von Karman street is concerned, our model studies only indicate what could happen and what are the parameters to measure. On the other hand this is the first experimentally relevant phenomenon we find which is sensitive to the above mentioned relationship.

III. **Work in progress.**

Since the beginning of our work there has been the problem of how to formalize the empirical implementation of the Lévy walk in lattice gas hydrodynamics. The investigator asserted in his first paper that the implementation was the equivalent in lattice gas hydrodynamics of a closure approximation. However this statement could not be shown explicitly, though we investigated the issue repeatedly with the collaboration of Stephane Zaleski in Paris.

We now believe we have made some major progress in this problem in the context of the BGK model. A modification of this model in a direction based on Lévy walk ideas leads - for turbulent channel flow - to results similar to the ones derived from the empirical Lévy walk implementation . What is interesting is that the numerical solution of the kinetic equation is computationally less efficient than the straightforward implementation. Our "empirical" algorithm thus appears to be an efficient way of implementing a modified kinetic equation which in the hydrodynamic limit leads - as we

are able to show - to the well-known closure approximation (zero equation model) of the Navier-Stokes equation!

IV. **Conferences**

F. Hayot attended the International Workshop on "Lévy flights and related phenomena in physics" (Nice, 1994), where he gave an invited talk on Lévy walks and lattice gas hydrodynamics.

Lukas Wagner attended the 5th International Conference on " Discrete models in fluid mechanics" (Princeton, 1994), and gave an invited talk on pressure and drag measurements in laminar and turbulent flows around a cylinder.

Lukas Wagner is attending the 1994 APS meeting on Fluid Mechanics (Atlanta,1994) where he will present our results for turbulent flows impinging on a cylinder.

REFERENCES.

1. F. Hayot, Phys. Rev A. **43**, 806 (1991), and J. of Stat. Phys. **68**, 557 (1992)

2. P. W. Bearman, J. Fluid Mech. **46**, 177 (1971)

Pressure in lattice Boltzmann simulations of flow around a cylinder

Lukas Wagner
Department of Physics
Ohio State University
Columbus, OH 43210

to appear in Physics of Fluids

Abstract

The expression for the pressure in lattice Boltzmann realizations of the Navier-Stokes equations involves compressibility effects. The pressure in 2-dimensional steady and unsteady cylinder flow is obtained numerically in a lattice Boltzmann scheme for the first time and compared with experimental and finite-difference results.

Since the discovery that lattice gases may be used to solve the Navier-Stokes equations[1] , related lattice Boltzmann (LB) equations have been written[2,3] which remedy many of their parent's shortcomings. In particular, the scheme of Chen *et al*[3] does not have an explicit velocity dependence of the pressure which the original lattice gas did. Moreover, the pressure is readily found with the noise-free LB schemes, while extracting pressure from noisy Boolean lattice gas simulations is a daunting prospect. While the theoretical validity of using LB equations to obtain numerical solutions to the Navier-Stokes equations has been verified by a number of studies, pressure in bluff-body flow has not been investigated yet.

It is useful to review briefly the derivation of the coarse-grained equations of motion, and thus of the pressure for LB methods. One begins the multiscale expansion of the site populations for the triangular lattice, f_i, about their equilibrium values, f_i^0, by writing the equilibrium values:

$$f_i^0 = (\rho - d_r)/b + \frac{\rho D}{bc2} c_{i\alpha} u_\alpha + \frac{D(D+2)\rho}{2bc^4} c_{i\alpha} c_{i\beta} u_\alpha u_\beta + \gamma u^2 \tag{1}$$

for the moving particles and

$$f_r^0 = d_r + \gamma_r u^2 \tag{2}$$

for the rest particles, with $\mathbf{c}_i$ the vector pointing in the ith lattice direction of modulus c, b the number of nonzero lattice vectors, $\rho = \Sigma_0^b f_i$, $\mathbf{u} = \Sigma \mathbf{c}_i f_i$, D the spatial dimension of the lattice, d_r a constant, and γ and γ_r related by $b\gamma + \gamma_r = -2\rho c^{-2}$. In reference [3], it was shown that by including the terms proportional to u^2 in (1) and (2), it is possible to eliminate a velocity dependence in the pressure which is present in a LB implementation of the original Frisch-Hasslacher-Pomeau lattice gas.

Upon performing the multiscale expansion $\partial_t \rightarrow \epsilon\partial_{t1} + \epsilon^2\partial_{t2} \ldots$, $\nabla \rightarrow \epsilon\nabla_1 + \ldots$ the equation for momentum transport to $O(\epsilon)$ is

$$\partial_t \Sigma c_{i\alpha} f_i^0 + \partial_\beta \Sigma c_{i\alpha} c_{i\beta} f_i^0 = 0 \tag{3}$$

$$\partial_t(\rho u_\alpha) + \partial_\alpha \Pi_{\alpha\beta} = 0 \tag{4}$$

where the leading approximation to the momentum flux density tensor is $\Pi_{\alpha\beta} = \frac{c^2}{D}\delta_{\alpha\beta}(\rho - d_r) + \rho u_\alpha u_\beta = \Sigma f_i c_{i\alpha} c_{i\beta}$, where the pressure (the isotropic part of $\Pi_{\alpha\beta}$) given by

$$p = (\rho - d_r)c^2/D. \tag{5}$$

Including terms of $O(\epsilon^2)$ changes $\Pi_{\alpha\beta}$ only by the addition of viscous terms, so (5) is unchanged. An alternative way to write (5) is the following: writing the momentum flux density with f_i (the actual populations of the lattice sites) instead of f_i^0, $\Pi_{\alpha\beta} = c^2 \Sigma c_{i\alpha} c_{i\beta} f_i$, gives for the pressure

$$p = (\rho - f_r - \rho u^2) c^2 / D, \tag{6}$$

which is equivalent to (5) when $f_r = f_r^0$. When f_r differs from f_r^0 (in time-dependent flows), the difference between (5) and (6) is still negligible— in the simulations presented here, on the order of 10^{-4} in units of dimensionless pressure p', $p' = (p - p_\infty)/\frac{1}{2}\rho U^2$.

To quantitatively test (6), we set a circular obstacle into a steady flow and examine the pressure. The boundary condition of steady flow far from the obstacle is approximated as follows: particles are injected with a distribution of uniform flow at the two boundaries of the system in the streamwise direction. In the direction perpendicular to the mean flow direction, periodic boundary conditions are used. A flow domain large enough for drag results accurate to 5% is used[4]. Since the drag is intimately related to the pressure near the cylinder, we estimate the error in pressure results due to finite size effects to be at most 5% also.

Figure 1 shows p' vs angle θ ($\theta = 0$ at the stagnation point) for a range of Re, at a distance of 4 lattice sites from the surface of the obstacle. The angle of minimum pressure as a function of Re appears identical with the finite-difference results for steady flow of Dennis[5], and consistent with Norberg's experiment[6], from which the result at $Re = 130$ is also shown . The maximum (minimum) values of the pressure shown in fig. 1 are consistently low (high) by as much as 15% in comparison with either experiment or finite difference methods, however. It is easy to see why this is so.

Namely, finding p at the surface of the obstacle in the LB method presents a difficulty not present with finite difference methods. A perfectly circular obstacle cannot be created on a regular lattice with no-slip boundary conditions. The edges of an approximation to a circle on a lattice have jagged edges, whose effect is discernible in the flow very near the obstacle. Evaluating the pressure at the surface of the obstacle does not yield a smooth $p(\theta)$; it is necessary to evaluate the pressure several sites (roughly a mean free path) away from the surface of the obstacle to obtain a curve that does not show discontinuities due to the lattice. Doing so introduces appreciable error both at the leading edge of the obstacle, and at the angle of minimum

pressure. Figure 2 compares the smooth curve at 4 lattice sites from the surface with the discontinuous curve at 1 lattice site from the surface. The difference between the two curves is most pronounced at the pressure extrema.

Figure 3 shows pressure at the stagnation point for the present LB simulations evaluated 1 site from the obstacle and for the finite difference simulations of Dennis[5]. Agreement is good, though the stagnation pressures from LB solutions are consistently smaller (by at most 6%) than Dennis' results.

Figures 4 and 5 show the pressure field away from the immediate neighborhood of the obstacle at $Re = 25$ and 75 respectively. Note the steep pressure gradient near the stagnation point and near the points of minimum pressure. The coarseness in the shape of the obstacle due to the lattice is visible in these figures. The low-pressure region behind the obstacle in figure 5 is a vortex that has just been shed. The Strouhal number for the vortex street shown in figure 5 is $St = D/\tau U = 0.162$, as compared to $St = 0.153$ for the experimental result[7], an error of 6%. This figure may be compared with the errors for St of $\leq 3.5\%$ in the exacting numerical study of Abarbanel *et al*[8].

While a detailed comparison of algorithmic efficiency with finite-difference and spectral methods was not undertaken, it is clear that LB methods share with finite difference and spectral methods the drawback of numerical instabilities for high Re imposed on insufficiently large computational domains[9]. On the other hand, work on grids with varying spatial resolution in LB methods[10], while very promising, is still in its preliminary stages.

I thank F. Hayot and Y. Pomeau for helpful discusions. This work was supported by the Department of the Navy, Office of Naval Research, under Grant No. N00014-92-J-1271, and benefitted from computer time at the Ohio Supercomputer Center.

References

[1] U.Frisch, B. Hasslacher, and Y. Pomeau, "Lattice-gas Automata for the Navier-Stokes equation," Phys. Rev. Lett. **56**,1505 (1986); U. Frisch, D. d'Humiéres, B. Hasslacher, P. Lallemand, Y. Pomeau, and J.-P. Rivet, "Lattice gas hydrodynamics in two and three dimensions," Complex Systems **1** 649 (1987)

[2] Y.H. Qian, D. d'Humières, and P. Lallemand, "Lattice BGK models for the Navier-Stokes Equation,"

Europhys. Lett. **17** 479 (1992)

[3] S. Chen, H. Chen, D. Martinez, and W. Matthaeus, "Lattice Boltzmann model for simulation of Magnetohydrodynamics," Phys.Rev. Lett. **67**, 3776 (1991); H. Chen, S. Chen, and W. H. Matthaeus, "Recovery of the Navier-Stokes equations using a lattice-gas Boltzmann method," Phys. Rev. A. **45** R5339 (1992)

[4] L. Wagner, Dependence of drag on a Galilean invariance-breaking parameter in lattice-Boltzmann flow simulations," Physical Review E **49** 2115 (1994)

[5] S.C.R. Dennis and G.-Z. Chang, "Numerical solutions for steady flow past a circular cylinder at Reynolds numbers up to 100," J. Fl. Mech. **42** 471 (1970)

[6] C. Norberg, "Measurements of pressure in cylinder flow," in *Bluff-Body Wakes, Dynamics, and Instabilities* H. Eckelmann, ed. IUTAM Symposium ser. 1994

[7] A. Roshko, "On the developmant of turbulent wakes from vortex streets," NACA TN-2913 (1953)

[8] S. S. Abarbanel, W. S. Don, D. Gottlieb, D. H. Rudy, and J. Townsend, "Secondary frequencies in the wake of a circular cylinder with vortex shedding," J. Fl. Mech **225** 557 (1991)

[9] J. Sterling and S. Chen, "Stability analysis of lattice-Boltzmann methods," Los Alamos preprint LA-UR:93-2103, ftp://xyz.lanl.gov:/nlin-sys/comp-gas/papers/9306/9306001

[10] R. Benzi, S. Succi, and M. Vergassola, "The lattice Boltzmann equation: theory and applications," Physics Rep. **222** 147 (1992)

Figure Captions

Figure 1. Solid curves are dimensionless pressure, $p' = (p - p_\infty)/\frac{1}{2}\rho U^2$ evaluated at a shell four sites from the obstacle's surface plotted versus angle for Reynolds numbers 6.4, 12.8, 25.6,51.2, 76.8 from bottom to top. Dashed curve is Norberg's experimental result at $Re = 130$. Each successive curve is offset by 0.5 for clarity. The pressure minima are marked with triangles.

Figure 2: Dimensionless pressure p' versus angle evaluated as in fig. 1 (line) and also on a shell one site from the surface of the obstacle at $Re = 25$ (points).

Figure 3. Dimensionless pressure at the stagnation point from Dennis and Chang[5] (open circles) and the present study (full circles).

Figure 4. Contour plot of dimensionless pressure at $Re = 25$. Dotted line is $p = p_{\text{inf}}$, with each contour corresponding to a step of $0.1p'$.

Figure 5. Contour plot of dimensionless pressure at $Re = 75$, contour lines defined as for fig. 3.

p'
-2.0
-1.0
0.0
1.0
2.0
3.0
4.0
-0.8
0.0
0.8
1.6
Θ − π/2

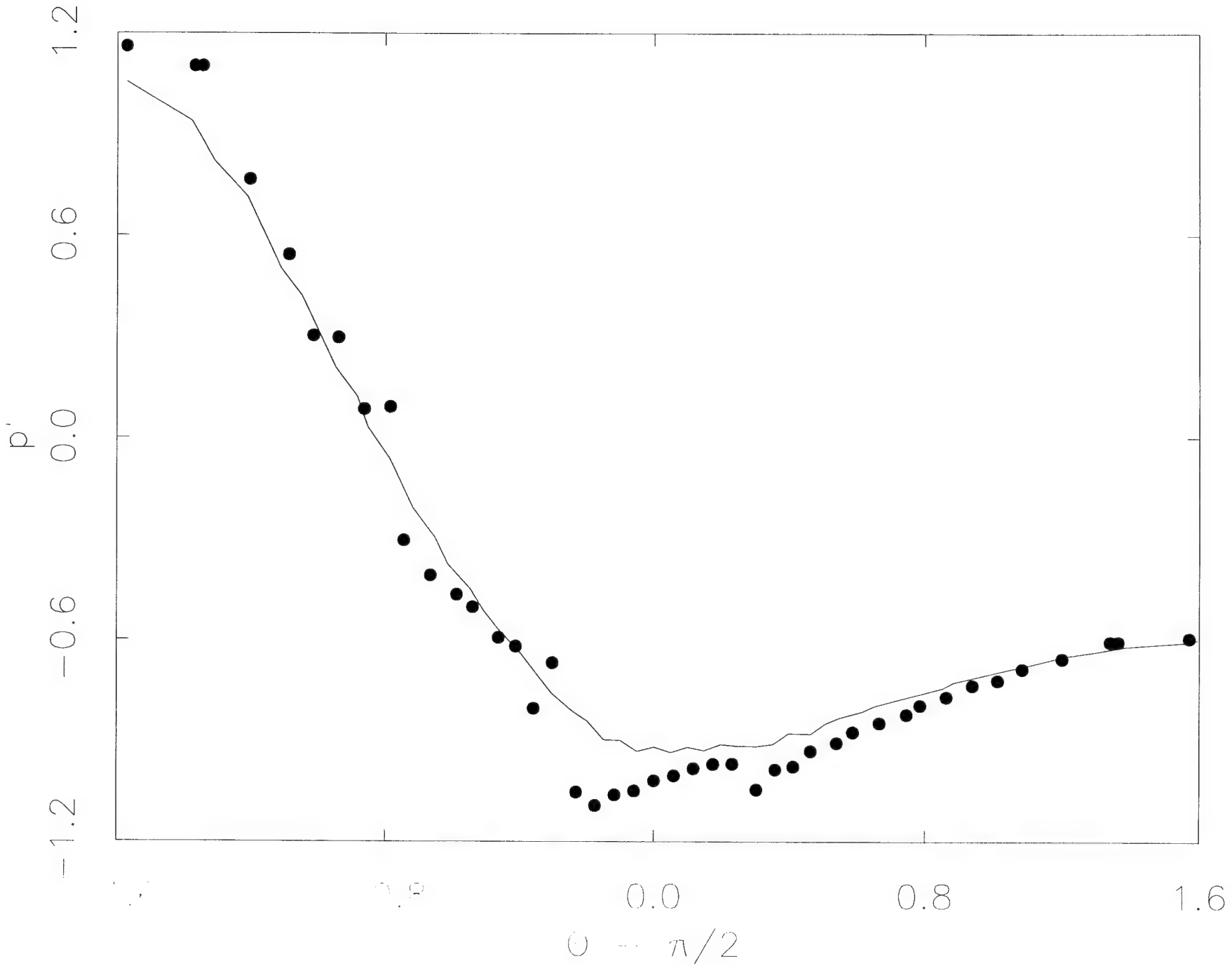
1.2
0.6
0.0
−0.6
−1.2
p'
0.0
0.8
1.6
θ — π/2

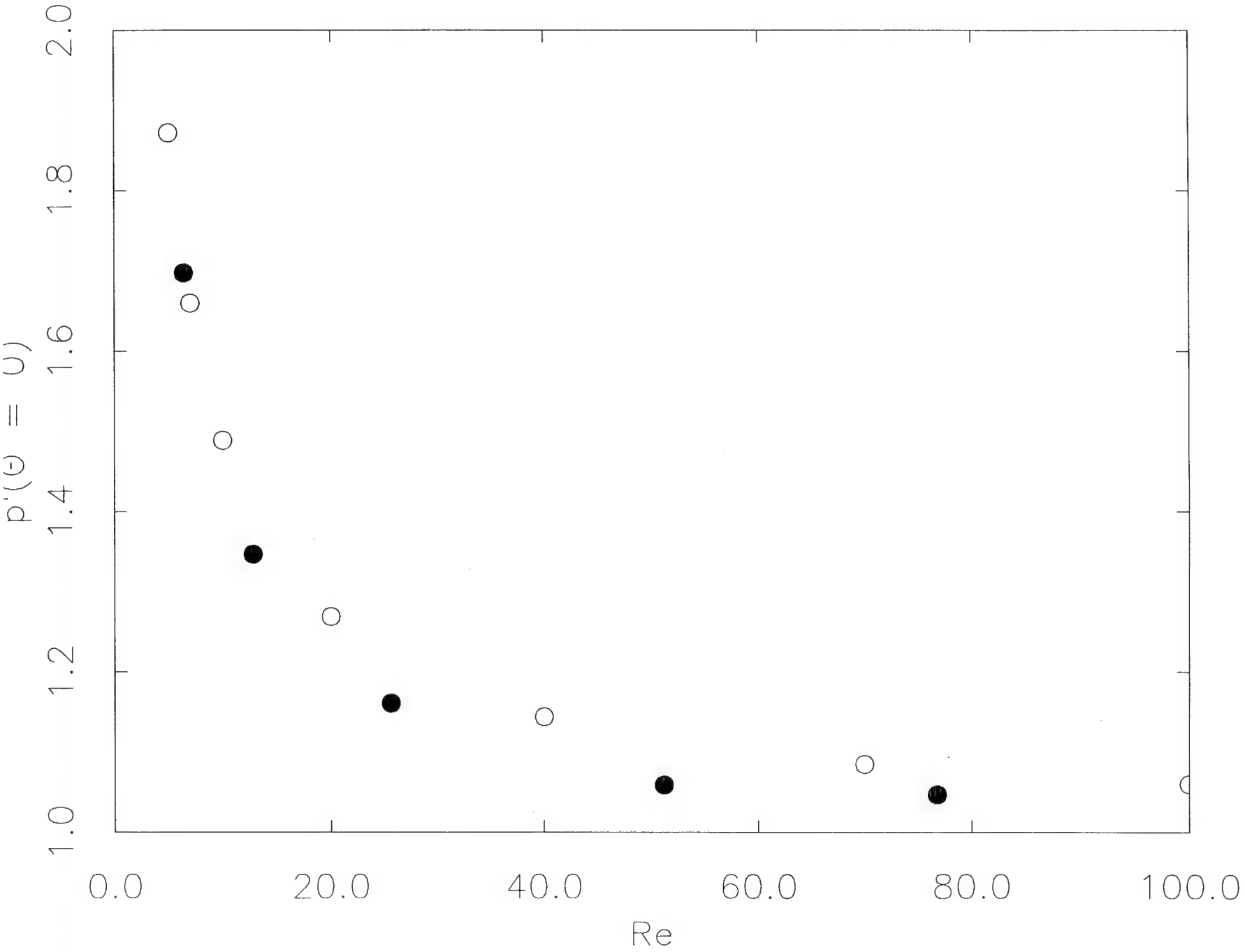
p'(Θ = 0)
2.0
1.8
1.6
1.4
1.2
1.0
0.0
20.0
40.0
60.0
80.0
100.0
Re

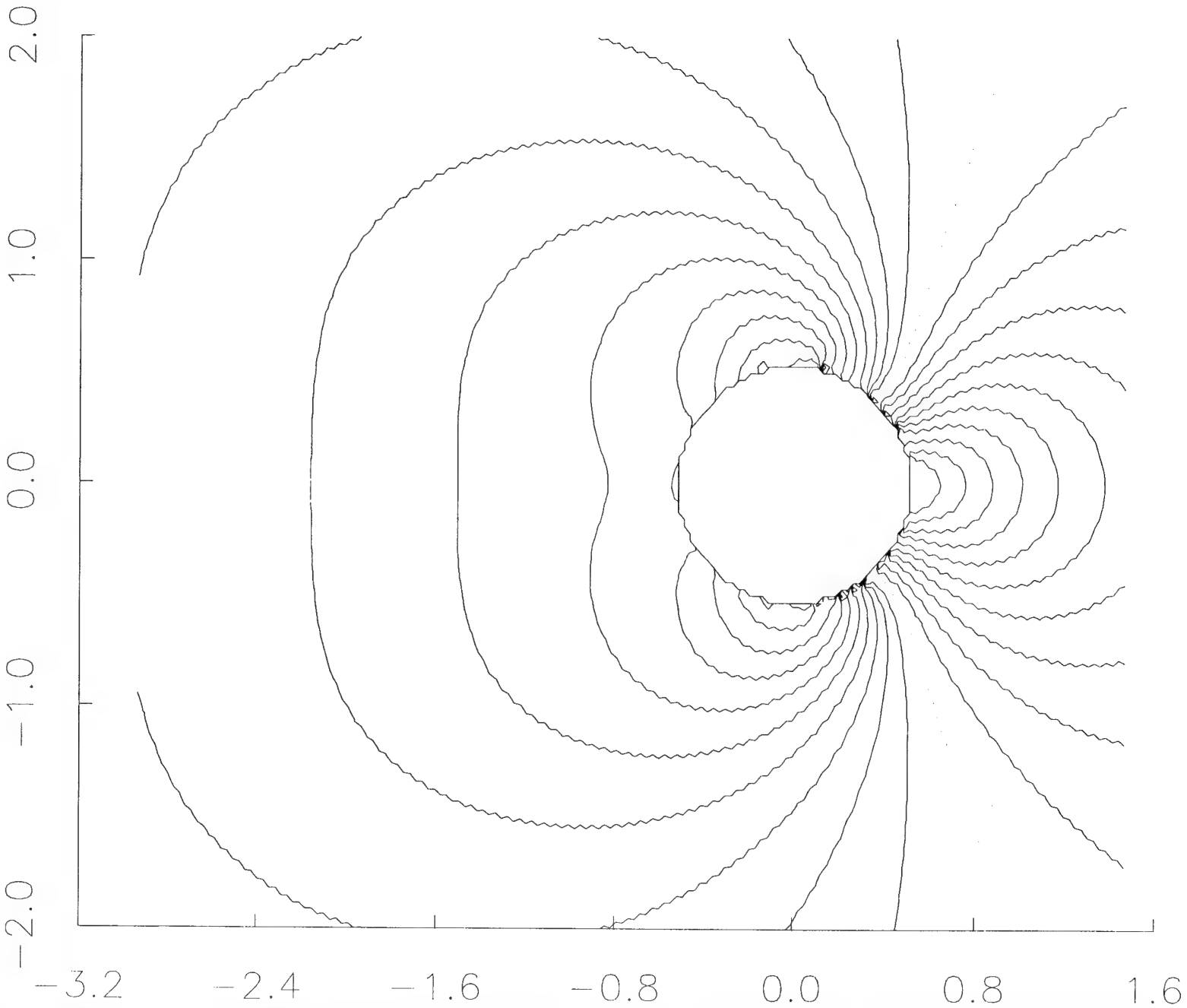
2.0
1.0
0.0
−1.0
−2.0
−3.2
−2.4
−1.6
−0.8
0.0
0.8
1.6

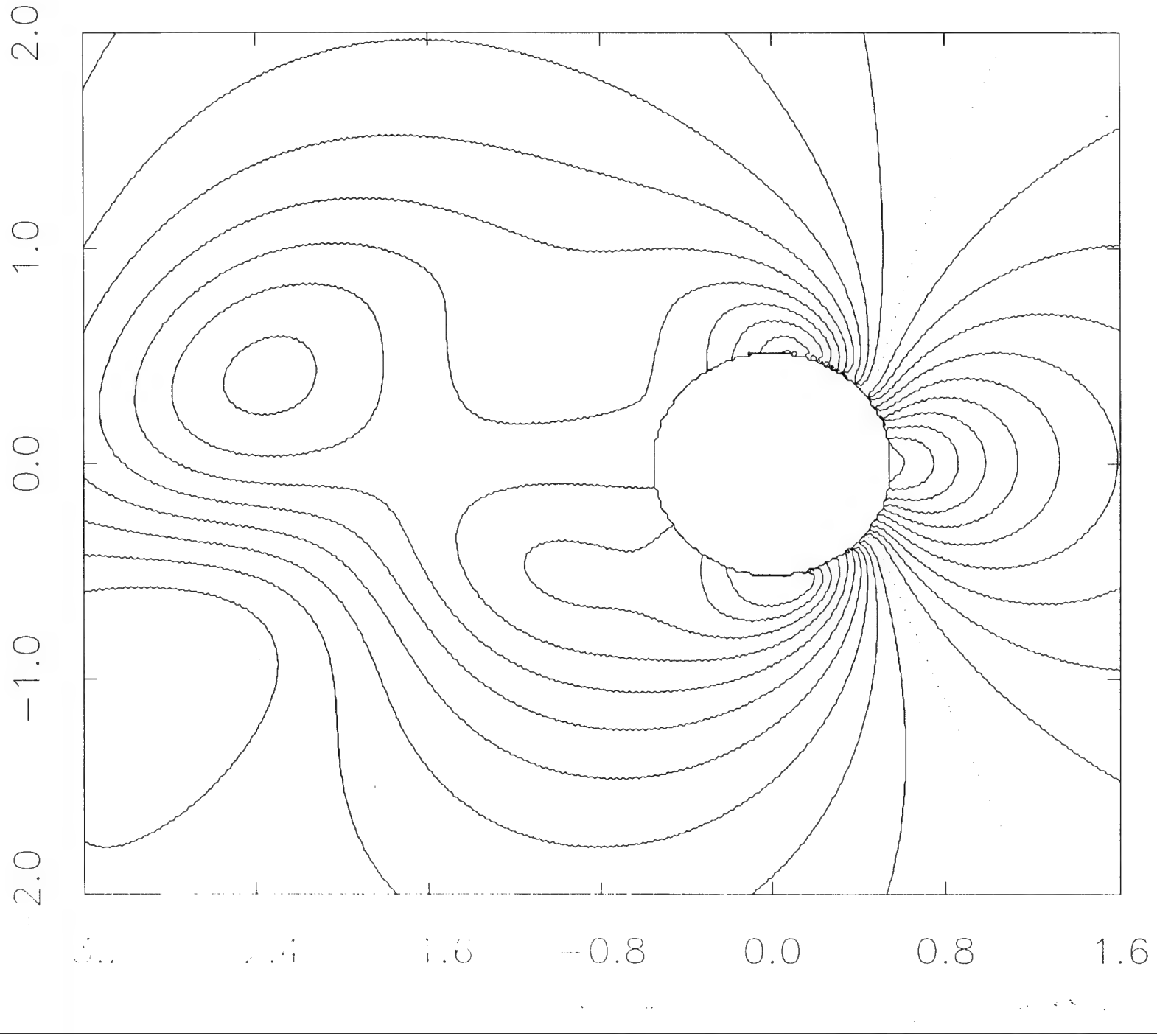
2.0
1.0
0.0
−1.0
2.0
1.6
−0.8
0.0
0.8
1.6

Lattice Boltzmann simulations of laminar and turbulent flow past a cylindrical obstacle

Lukas Wagner and Fernand Hayot

Department of Physics

Ohio State University

Columbus, OH 43210

Abstract

We present lattice Boltzmann simulations of flow past a cylindrical obstacle. We are interested in the effect of turbulence in the incident flow on the coherence of the von Karman street.

Our study is based on the Lévy walk model of turbulence in a lattice Boltzmann model. We discuss pressure around the cylinder in the laminar and turbulent regimes, as well as the dependence of the von Karman street on the analogue of integral scale in our model.

The lattice-Boltzmann (LB) scheme of Chen *et al* [1] is an efficient way of obtaining numerical solutions to the Navier Stokes equations. We use this LB scheme to investigate laminar flow around a cylinder, and also to model the effect of turbulence in the incident flow, with particular attention on the pressure, drag, and coherence of the von Karman street. As a model for incident turbulence, especially the enhanced transport of momentum into and out of the wake, we use an exchange model well suited to implementation in an LB scheme.

We mimic momentum transport by an eddy of size ℓ by exchanging the populations of two randomly chosen sites separated by ℓ, with ℓ chosen with a probability $p(\ell) \propto \ell^{-1.3}$ for all results presented here. In agreement with the discussion of Schlesinger *al* [2], we associate a waiting time with each length ℓ. Since the waiting time is the reciprocal of the frequency of jumps of a particular length, the distribution of waiting times is set by the dependence of the number of exchanges, $N(\ell)$, on ℓ. We use here $N(\ell) \propto N_0 - \ell$.

We implement this model in 2-dimensional flow past a circular obstacle. The obstacle is set into a channel with uniform velocity U at the boundaries in the streamwise direction x, and periodic boundaries in the transverese y direction. A more precise description of the flow geometry may be found elsewhere [3,4]. This is an extension of our previous study of a Lévy walk based model of turbulence in a boolean implementation of channel flow [5]. In addition to being able to resolve more precisely the velocity field, we are able to investigate the pressure in this LB implementation.

There are two basic length scales when the LB model with exchanges is used to model cylinder flow with incident turbulence. One is ℓ_{max}, the maximum allowed exchange length, which sets a length scale for the turbulent exchanges. ℓ_{max} in our model plays the role of the integral scale in experimental studies. The second length scale in flow past an obstacle is just the obstacle diameter, D; the ratio of these two length scales is clearly a useful parameter in characterizing the flow.

One difficulty in finding pressure at a surface in the LB method not present with finite difference methods is that a perfectly circular obstacle cannot be created on a regular lattice

with no-slip boundary conditions. The edges of an approximation to a circle on a lattice are jagged, which produces discernible effects in the flow very near the obstacle. Evaluating the pressure at the surface of the obstacle does not yield a smooth $p(\theta)$; it is necessary to evaluate the pressure several sites (roughly a mean free path) away from the surface of the obstacle to obtain a curve that does not show discontinuities due to the lattice. Doing so introduces appreciable error both at the leading edge of the obstacle, and at the angle of minimum pressure. Results presented in figs. 1 and 9 are thus for pressure evaluated 4 lattice sites away from the surface of the obstacle.

The pressure in *laminar* flow as calculated in the LB scheme without exchanges agrees with experiment [6] and finite difference studies[7,8]. Figure 1 depicts the pressure near the obstacle surface as a function of angle at various Re.

Figures 2 and 3 show the pressure field without and with exchanges respectively at a mean-flow Re of 76.8. The symmetric pressure field shown in fig. 3 suggests that in this case, the von Karman street is destroyed by incident turbulence. This is easily verified by inspecting the dependence of $v(3.5D, 0)$, the component of the velocity perpendicular to the mean flow at a position 3.5 diameters downstream of the obstacle's center, on ℓ_{max}, which is shown in fig. 4. The inset shows how the time series of $v(3.5D, 0)$ changes character with increasing exchange length; the intermittent intervals of regular oscillation in the velocity become rarer with increasing exchange length.

An examination of u, the streamwise velocity suggests a simple explanation for why the exchanges suppress the von Karman street. Figures 5 and 6 show contours of constant u with no exchanges and with $\ell_{max} = 7D$, respectively. The wake behind the obstacle is much shorter with incident turbulence than without. Both the shortened wake and the absence of vortex shedding are explained by the effect of the enhanced momentum transport provided by the Lévy distributed exchanges. The exchanges (and the eddies which they model) transport momentum between the slowly moving fluid behind the obstacle and the fast moving fluid to either side. The net effect is to accelerate the fluid behind the obstacle, thus shortening the wake. The same mechanism of enhanced momentum transport affects

the region immediately behind the obstacle, where vortices form before they are shed in the absence of turbulence. Sufficiently many exchanges between a nascent vortex and any other region in the flow suppress the formation of the vortex, and thus there can be no vortex street. Bearman, in his experimental study on the effects of incident turbulence on flow around flat plates at much higher mean-flow Re [9], also states that the main effect of turbulence in the incident flow is to the exchange of momentum between flow inside and outside of the wake.

The simple picture that if ℓ_{max}/D is sufficiently large, the von Karman street will be destroyed, is complicated but essentially unaltered by spectral analysis and an investigation of spatial correlation in the flow. Figure 7 shows that the power spectrum of the velocity behind the obstacle $v(\omega)v^*(\omega)$ retains a peak near the Strouhal frequency even with $\ell_{max} = 7D$, though the velocity oscillations are so small that they do not seem to be due to translating vortices. The shedding of a vortex produces strong spatial correlations in the flow. In particular, the quantity $c(x) = \langle \Delta v(x,0)\Delta v(x,D/2)\rangle$ varies very slowly with x in laminar flow, as may be seen in fig 8. For $\ell_{max} \geq 3D$, however, the correlation falls of sharply with increasing distance from the obstacle. If the correlation in velocities arose as a consequence of spatially coherent vortices being convected upstream, the correlation should change only as the vortices diffuse away. The transverse velocity does not show such a slowly changing correlation with long exchanges— it is larger in magnitude near the obstacle and shows stronger spatial correlation there also. Such behavior might be due to oscillation of the vestigial wake. An experimental study [10] performed in turbulent shear flow past a cylinder, at lower mean flow Re than Bearman's investigation, supports the qualitative conclusion that turbulence with a large integral scale disrupts vortex shedding.

The effect of the momentum exchanges on the velocity field provides a ready interpretation for the changes in the pressure near the obstacle, pictured in figure 9. The pressure behind the obstacle is smaller with turbulence than without, and the pressure in front is larger. The smaller pressure behind the obstacle is a consequence of the weaker backflow in the wake, that is, of the enhanced momentum exchange between the wake and its sur-

roundings. Similarly, exchanges tend to reduce v upstream from the obstacle, thus raising the pressure there. We have checked that the pressure with exchanges shown in fig. 9 is insensitive to the form of $N(\ell)$

The drag, shown in fig. 10 as a function of ℓ_{max}/D reflects these changes in the pressure. For small ℓ, the drag reflects the suppression of the vortex street and the enhanced transport of momentum by the Lévy distributed exchanges. Once ℓ_{max}/D becomes large enough, increasing the size of the largest exchanges is no longer significant, so the change in drag only reflects the slow increase in the probability of long exchanges with further increases in ℓ_{max}. Exactly how large depends on the choice of $N(\ell)$. Our results for how turbulence in the incident flow affects pressure and drag are in qualitative agreement with Bearman's results for flat plates [9].

To conclude, we have implemented a Lévy walk-based model for incident turbulence in channel flow and verified that vortex shedding is suppressed by incident turbulence of large enough length scale. We have also qualitatively reproduced experimental results on the effect of incident turbulence on drag and the suppression of vortex shedding at low *Re* by turbulence with a length scale large compared to cylinder diameter.

This work was supported by the Department of the Navy, Office of Naval Research, under Grant No. N00014-92-J-1271, and benefitted from computer time at the Ohio Supercomputer Center.

References

[1] H. Chen, S. Chen, and W. H. Matthaeus, Phys. Rev. A. **45** R5339 (1992).

[2] M.F. Schlesinger, B. J. West, and J. Klafter, Phys. Rev. Lett. bf 58, 1100 (1987).

[3] Lukas Wagner, Phys. Rev. E **49** 2115 (1994).

[4] Lukas Wagner, Physics of Fluids A, to be published.

[5] F. Hayot and L. Wagner, Phys. Rev. E **49** 470, (1994).

[6] C. Norberg, in *Bluff-Body Wakes, Dynamics, and Instabilities* H. Eckelmann, ed. IUTAM Symposium ser. 1994.

[7] S.C.R. Dennis and G.-Z. Chang, J. Fl. Mech. **42** 471 (1970)

[8] S. S. Abarbanel, W. S. Don, D. Gottlieb, D. H. Rudy, and J. Townsend, J. Fl. Mech **225** 557 (1991)

[9] P.W. Bearman, J. Fluid Mech. **46**, 177 (1971).

[10] M. Kiya and H. Tamura, J. of Fluids Eng. **111**, 126 (1989).

Figure Captions

Figure 1. Solid curves are dimensionless pressure, $p' = (p - p_\infty)/\frac{1}{2}\rho U^2$ evaluated at a shell four sites from the obstacle's surface plotted versus angle for Reynolds numbers 6.4, 12.8, 25.6,51.2, 76.8 from bottom to top. Dashed curve is Norberg's experimental result [6] at $Re = 130$. Each successive curve is offset by 0.5 for clarity. The pressure minima are marked with triangles.

Figure 2. Contour plot of dimensionless pressure at $Re = 75$. Dotted line is $p = p_{\rm inf}$, with each contour representing a step of $0.1p'$.

Figure 3. Contour plot of dimensionless pressure at $Re = 75$ with Lévy model of incident turbulence; $\ell_M = 7D$, contour lines defined as for fig. 2.

Figure 4. Peak transverse velocity measured at a station 3.5 diameters downstream from the obstacle center, $v(3.5D, 0)$. plotted against maximum exchange length. Inset shows time series of $v(3.5D, 0)$ for $\ell_{max} = 2D$ (dots) and $3D$ (line) showing the intermittency of the periodic oscillations.

Figure 5. Contour plot of u/U, the nondimensional streamwise velocity component for laminar flow at $Re = 76.8$. The dotted contour is $u = 0$, and shows the extent of the wake. Each contour line corresponds to a step of $u = U/6$

Figure 6. Contour plot of u/U, the nondimensional streamwise velocity component for laminar flow at mean-flow $Re = 76.8$. with $\ell_{max} = 7D$. Contours defined as in fig. 5. Note the shortened wake and the slower flow around the obstacle.

Figure 7. Power spectra of $v(3.5D, 0)$ for $\ell_max = 2D$ (solid line), $3D$ (dashed line), $5D$ (dash-dotted line), and $7D$ (dotted line). All curves have been rescaled to have similar maxima.

Figure 8. Correlations in v at two positions downstream from the obstacle. The change in c indicates that the peak near the Strouhal frequency is not due to vortex shedding.

Figure 9. Pressure as a function of angle in laminar flow (solid line) and with incident turbulence with $\ell_{max} = 7D$, dash-dotted line.

Figure 10. Drag plotted as a function of ℓ_{max}/D. The insets show time series of the drag in laminar flow at $Re = 76.8$ and for flow with incident turbulence with $\ell_{max} = D$. Even the weakest turbulence, which still leaves the von Karman street intact, is strong enough to mask the small-amplitude oscillations the drag undergoes as vortices are shed.

p'
-2.0
-1.0
0.0
1.0
2.0
3.0
4.0
0.0
0.8
1.6
Θ - π/2

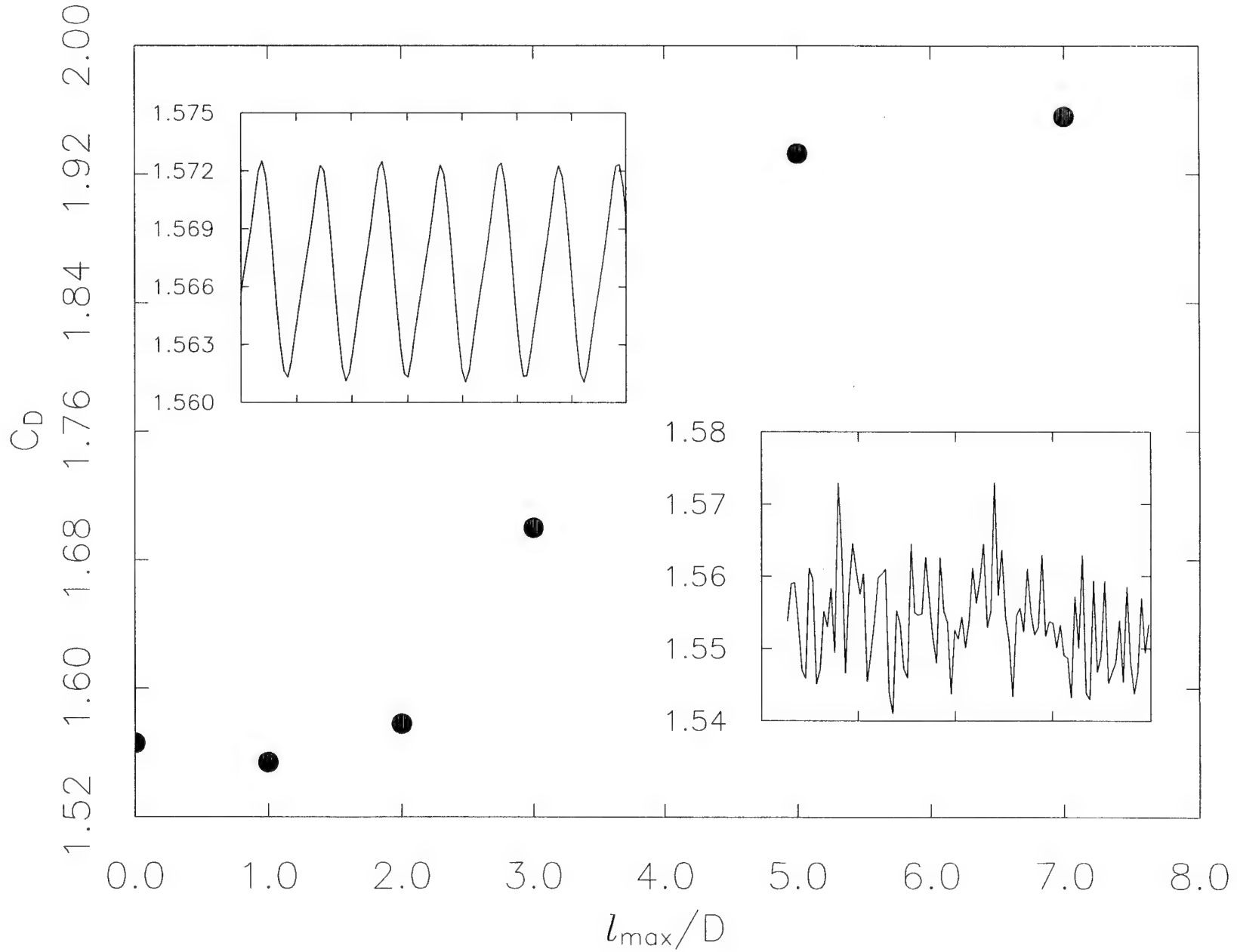
2.00
1.92
1.84
1.76
1.68
1.60
1.52
C_D
1.575
1.572
1.569
1.566
1.563
1.560
1.58
1.57
1.56
1.55
1.54
0.0
1.0
2.0
3.0
4.0
5.0
6.0
7.0
8.0
l_{max}/D

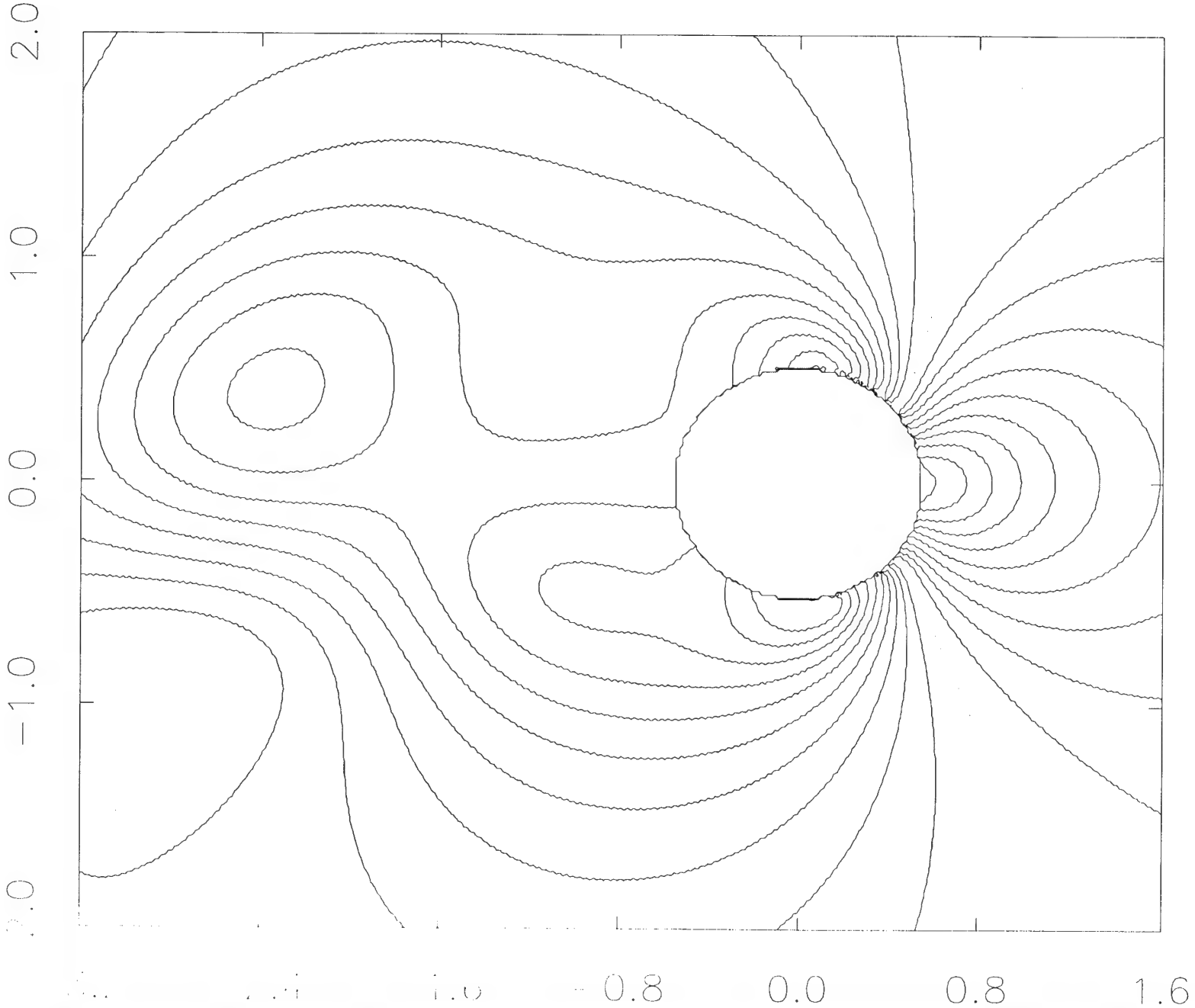
2.0
1.0
0.0
−1.0
−0.8
0.0
0.8
1.6

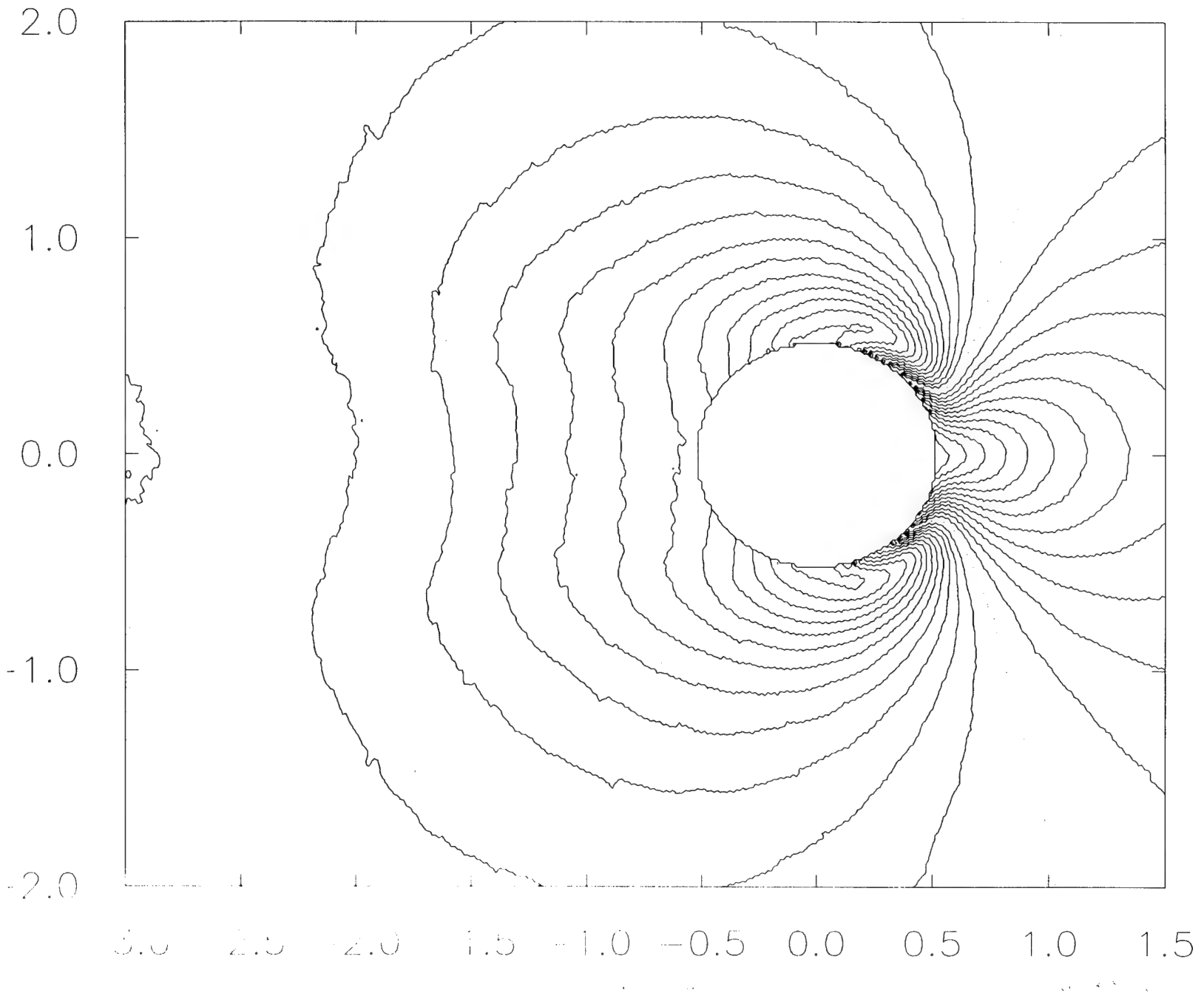
2.0
1.0
0.0
-1.0
-2.0
-1.0
-0.5
0.0
0.5
1.0
1.5

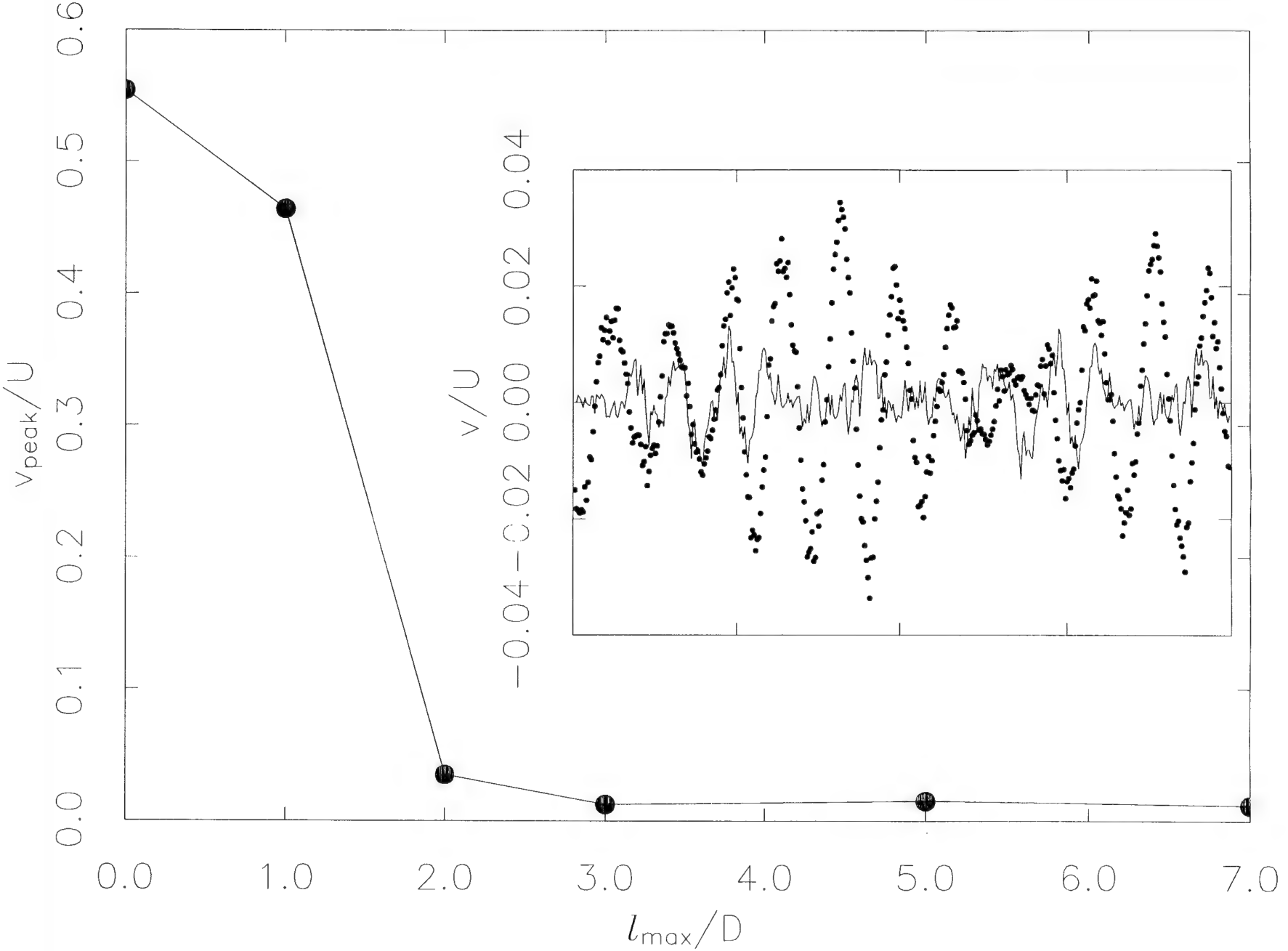
0.0
0.1
0.2
0.3
0.4
0.5
0.6
v_{peak}/U
0.0
1.0
2.0
3.0
4.0
5.0
6.0
7.0
l_{max}/D
v/U
−0.04
−0.02
0.00
0.02
0.04

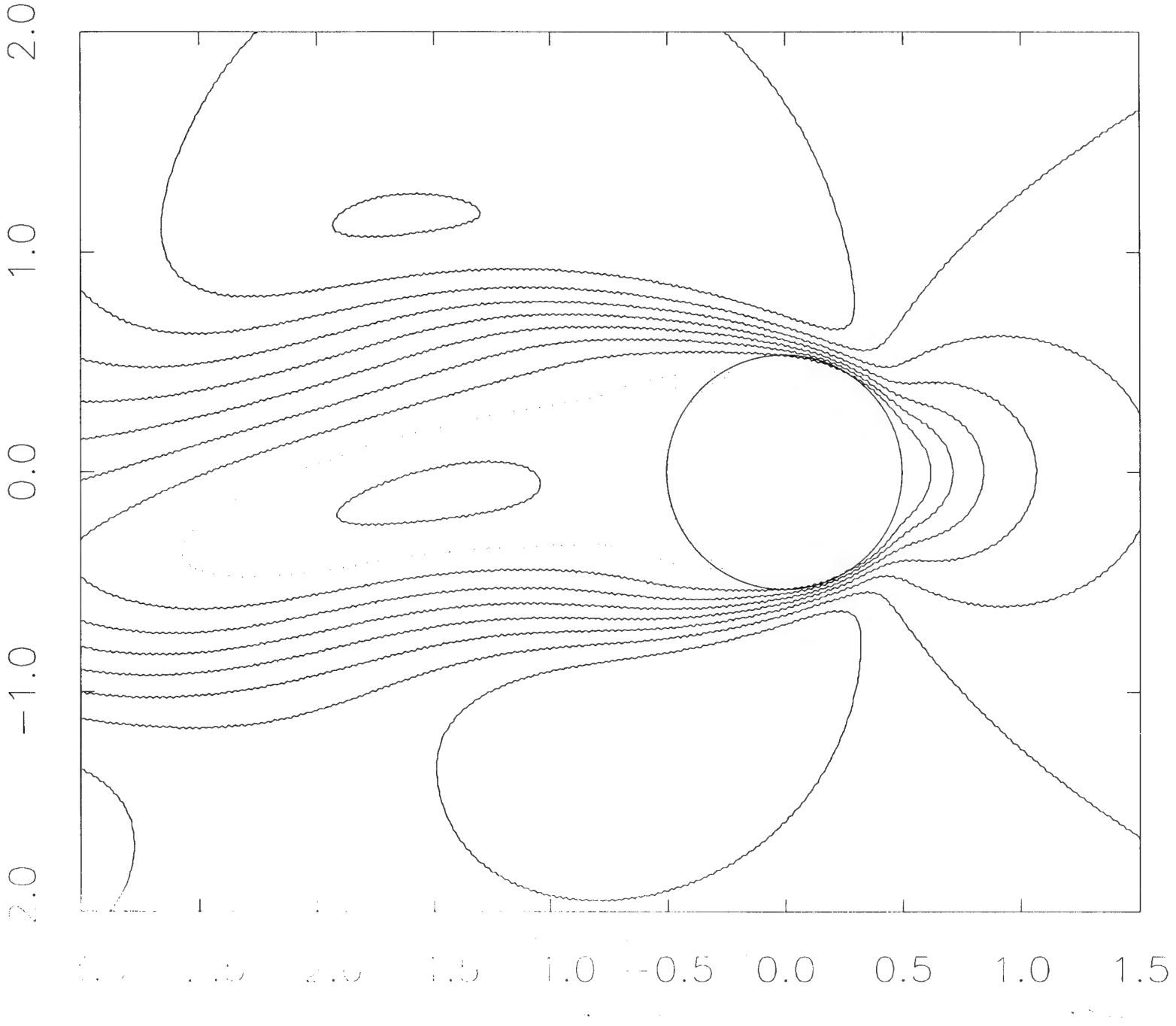
2.0
1.0
0.0
−1.0
2.0
1.0
−0.5
0.0
0.5
1.0
1.5

2.0
1.0
0.0
−1.0
−2.0
−3.0
−2.5
−2.0
−1.5
−1.0
−0.5
0.0
0.5
1.0
1.5

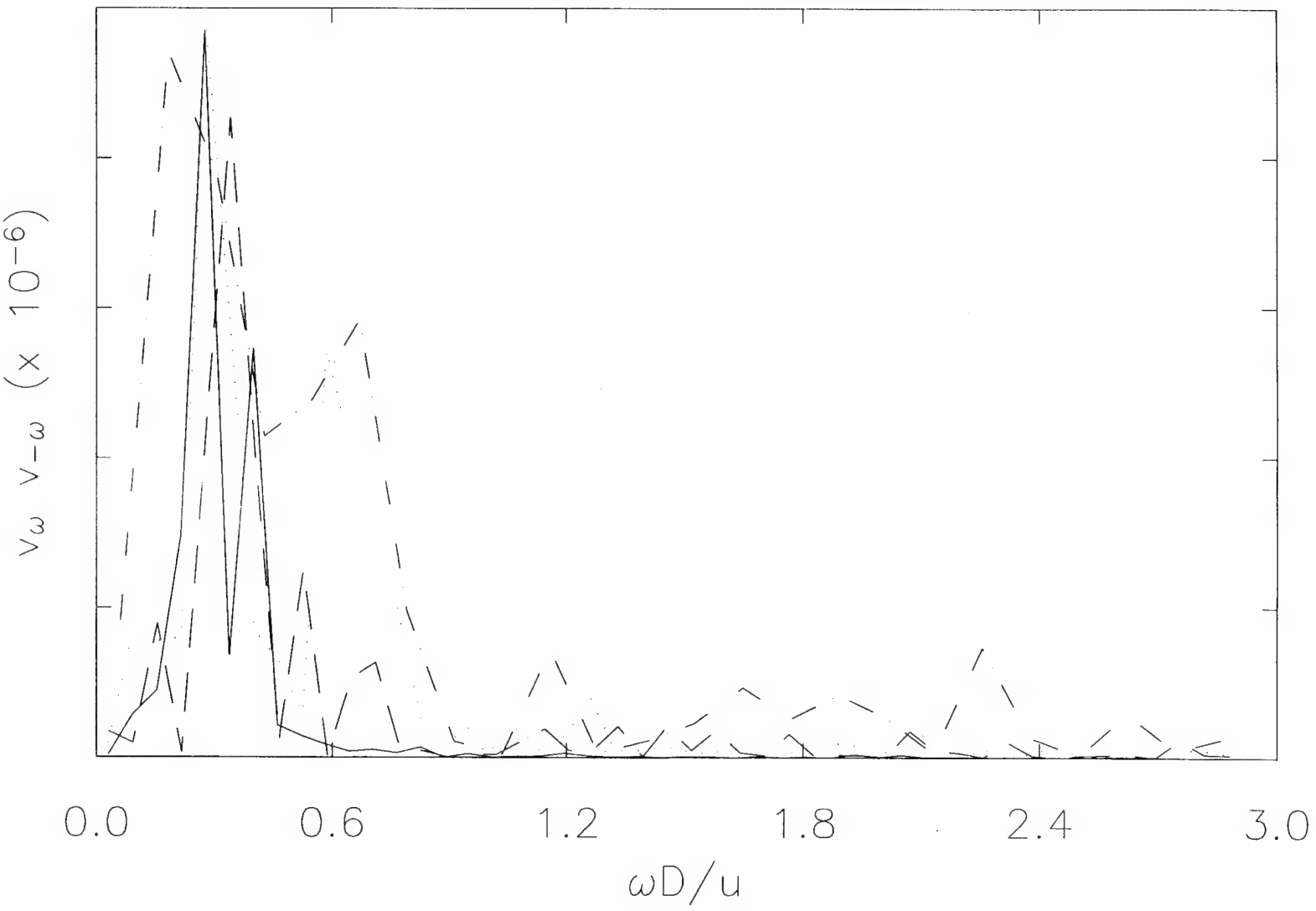
$v_\omega\ v_{-\omega}$ (x 10^{-6})
0.0
0.6
1.2
1.8
2.4
3.0
$\omega D/u$

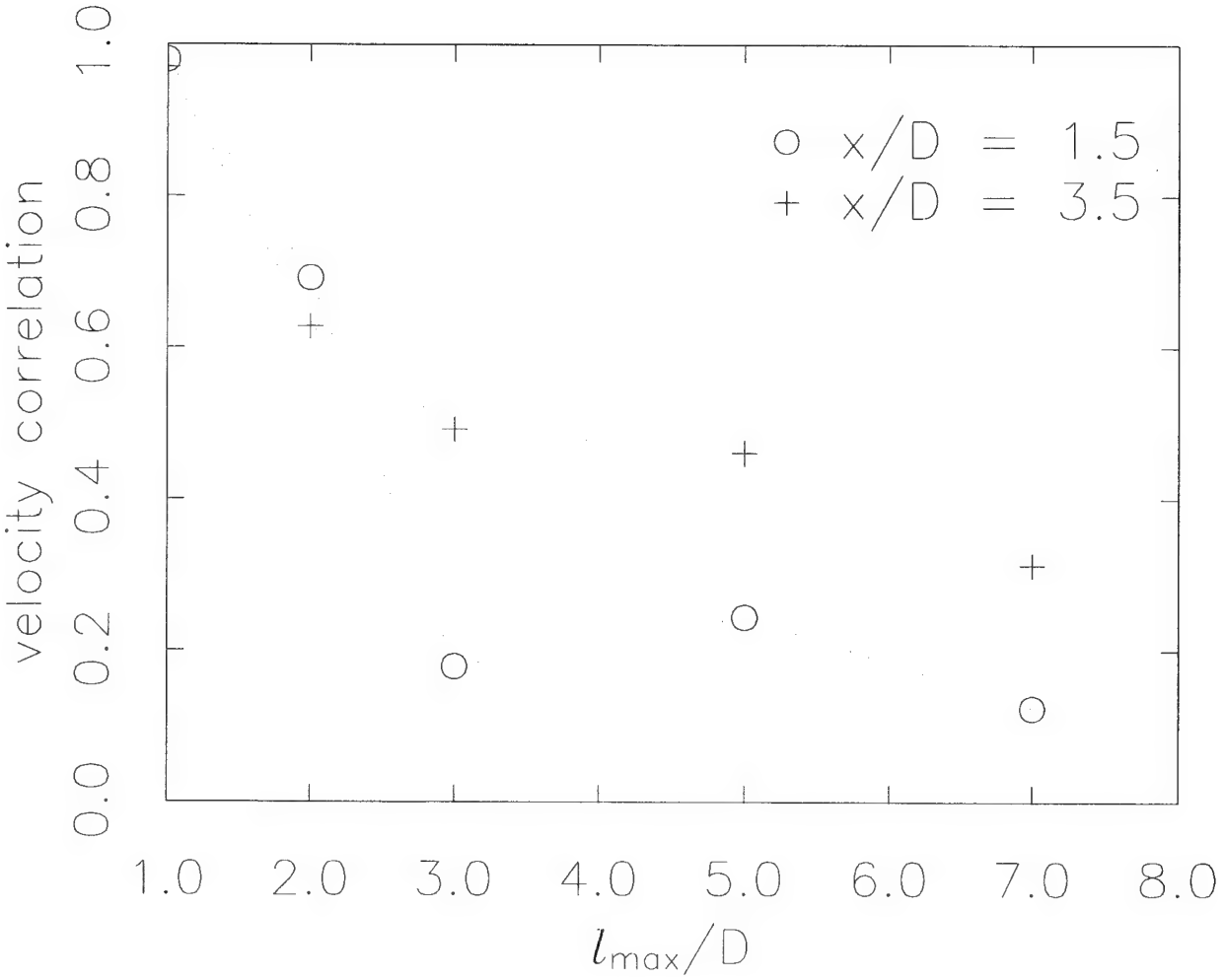
velocity correlation
0.0
0.2
0.4
0.6
0.8
1.0
o x/D = 1.5
+ x/D = 3.5
1.0
2.0
3.0
4.0
5.0
6.0
7.0
8.0
l_{max}/D

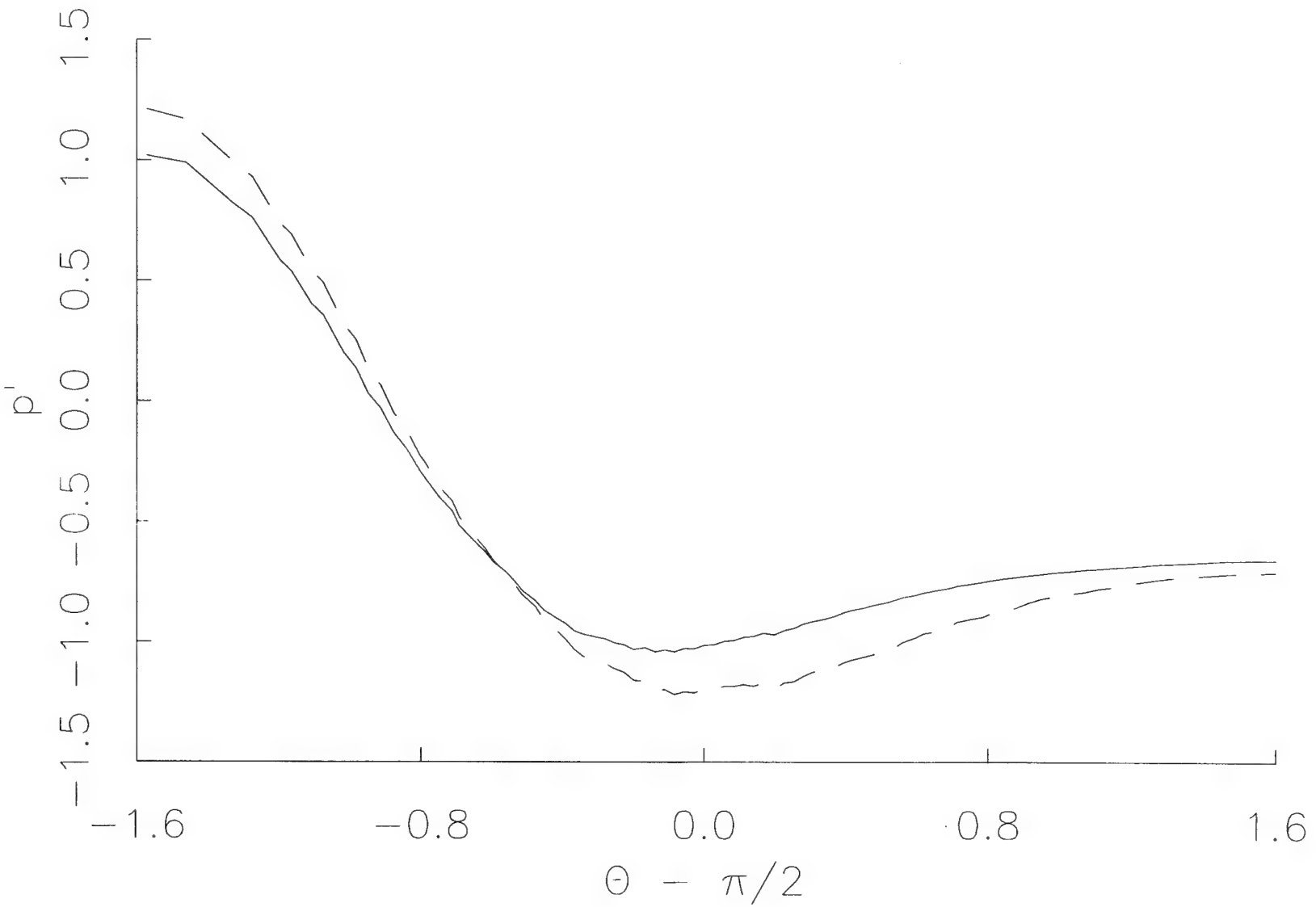
p'
1.5
1.0
0.5
0.0
−0.5
−1.0
−1.5
−1.6
−0.8
0.0
0.8
1.6
θ − π/2

Lévy walks and lattice gas hydrodynamics

F. Hayot and L. Wagner

Department of Physics, The Ohio State University, Columbus, Ohio 43210

Abstract. We describe an algorithmic implementation of Lévy walks in lattice gas hydrodynamics, which we use to discuss the effects of turbulence in flow around an infinite cylinder. We describe our results on pressure around the cylinder, drag, and coherence of the Von Karman vortex street.
Keywords. Lévy walk, lattice gas hydrodynamics, turbulence, flow around a cylinder.

1. Introduction.

We wish to discuss an implementation of the main features of Lévy walks in lattice gas hydrodynamics[1]. The main features are those highlighted in the paper by Shlesinger,West and Klafter[2] in a description of enhanced turbulent diffusion (Richardson's law[3]). The situation we will study is turbulent channel flow, in particular the case where turbulent flow is incident on an infinite cylinder. We thus limit ourselves to two dimensional situations. Before describing the implementation, we need to briefly recall the main features of lattice gas hydrodynamics.

Lattice gas hydrodynamics is a fluid mechanical description at the microscopic or kinetic level. There are two different versions, a Boolean one and one which takes the form of a Boltzmann equation. The first deals with integer numbers, and averaging over lattice regions is required in order to describe real number fields such as fluid velocity. The implementation is purely algorithmic. How and why, after coarse graining, macroscopic fluid behavior emerges, has been amply shown[4](in the low Mach number limit). The second one operates at a less deep microscopic level, deals with real numbers, and amounts to solving a Boltzmann equation numerically. Since in this case no coarse graining takes place, there is no intrinsic statistical noise, which is a great advantage when one aims at obtaining quantitative results.

2. Lattice gas hydrodynamics.

Let us now describe the Boolean version of lattice gas hydrodynamics, though the results described later will make use of a Boltzmann equation. The reason for doing so is that the introduction of Lévy walks is somewhat easier to describe in the Boolean case. The lattice gas is a collection of point particles, which move about from site to site on a two dimensional hexagonal regular lattice. At each site there are six possible directions for a particle to move into. In one unit of

time the particle moves a distance of one unit between sites. Thus, though the direction of velocity can change, its magnitude is fixed at unity. Besides moving in the direction indicated by their velocities, at each time step also particles, at the same site, can undergo two-, three- or four- particle collisions, which are momentum conserving, and conserve the number of particles[4]. (Energy conservation is trivial in the simple models with moving particles we consider, because it is equivalent to particle number conservation.) The algorithm is such at at any given time step, at any given site, there can be only one or no particle moving in a given direction. The configuration of particles can therefore be represented by a set of binary numbers. This is the Boolean character, which assures numerical stability, but requires coarse- graining for defining velocity and density fields.

The simplest Boltzmann model is a discrete version of the so- called BGK (Bhatnagar, Gross, Krook) model[5], for which the evolution equation is the following:

$$f_i(\mathbf{x}+\mathbf{c_i},t+1)-f_i(\mathbf{x},t)=(-1/\tau)(f_i(\mathbf{x},t)-f_i^0(\mathbf{x},t)), \qquad (1)$$

Here $i = 1,...,6$ numbers the six directions on the hexagonal lattice, of unit vectors denoted $\mathbf{c_i}$, and f_i is the number density of particles in the i^{th} direction. The coefficient τ, which will be of order unity is the relaxation time to the local distribution f_i^0, which is chosen appropriately for our purposes, as a function of the local macroscopic density and velocity. The model we are using contains also rest particles which satisfy a separate equation with a separate local distribution function. The details of the model can be found in reference 6, where it is made clear which choices are made for the local functions and why these are advantageous. The kinematic viscosity in the model is linearly related to τ. We have used the model extensively to discuss drag and pressure distribution for flow around a cylinder at Reynolds numbers of the order of 100, and found quantitative agreement with experiment[7].

3. Lévy walk implementation.

3.1. *Description.*

Let us now describe how the Lévy walk part is transplanted into the Boolean algorithm of lattice gas hydrodynamics. The two principal features of the Lévy walk we retain is that there is exchange of momentum over large distances (the probability density distribution falls off algebraically at large distances), and that there is a characteristic time associated with each exchange with is distance dependent. First recall that an update in lattice gas hydrodynamics is a combination of both a translation of particles into the directions of their velocity vectors followed by a momentum and energy conserving collision, if allowed. In between two successive updates the Lévy walk part of the algorithm proceeds as follows.

Imagine pressure driven channel flow. A distance l is drawn from an algebraic probability density distribution of the form

$$p(l) \propto l^{-z} \qquad (2)$$

The value of z is 1.35 for the results reported here, and is basically the only parameter. If z gets too large, large distances contribute less, and therefore the exchanges do not change the laminar flow.

Once l is drawn, a point S is uniformly chosen through the channel, and the particle configurations at two sites, at equal distances l from S in, say, a direction transverse to the flow are exchanged. This operation corresponds to momentum exchange over a distance of $2l$, such that overall momentum is conserved. For a chosen l, the number of exchanges, or correspondingly the number of points S chosen, is made to depend on the value of l. The algorithm is such that the larger l is, the fewer exchanges over distance $2l$ take place. For a given l, as many different points S are drawn until the required number of exchanges has taken place. (If S is too close to the boundary for the exchange of chosen l to take place, a new S is drawn.) We typically use for the number of exchanges a linear dependence on l, of the form $N(l) = N_0 - l$. Since the Lévy walk implementation takes place within one update time, the characteristic time associated with each distance l is inversely proportional to the number of corresponding exchanges. In other words, as required, the characteristic time associated with long jumps is longer than for small jumps.

For the BGK model (equation (1)) the Lévy walk implementation is similar. The system is updated at time intervals one unit apart according to equation (1), and within each such time interval the Lévy walk algorithm is implemented, namely choices of l (and thus $N(l)$), and of positions S are made.

3.2. *Discussion.*

The Lévy walk exchanges act to maintain the system in a stationary out of equilibrium state. They achieve this because they take place on time scales smaller than the relaxation time τ. Though the long range part of the exchanges might be represented in, say equation (1), through the introduction of some nonlocal long range force, there is also the characteristic , length dependent, time associated with each exchange. The time over which quantities in equation (1) evolve is of order unity, and the Navier- Stokes equations are obtained, at long times and large scales, through a Chapman- Enskog expansion, for which there is local momentum and particle number conservation. However, in the algorithm, the exchanges take place on time scales smaller than the unit update time. On these time scales there is only global momentum conservation, no longer a local one. (We have checked that the particle number i. e. mass transport which our procedure entails has a negligible effect.) We do not know how to formalize this.

4. Results and comparison with experiment

The experimental situation concerns flow impinging on an infinite cylinder, when the flow is turbulent. Turbulent intensity is of the order of several percent, as measured by the ratio of fluctuating to average velocities. The other quantity characterizing the turbulence is the integral scale, and its ratio to cylinder diameter. To model this situation, we implement the Lévy walk algorithm, described above in the Boolean case, for the Boltzmann model given by equation (1). What

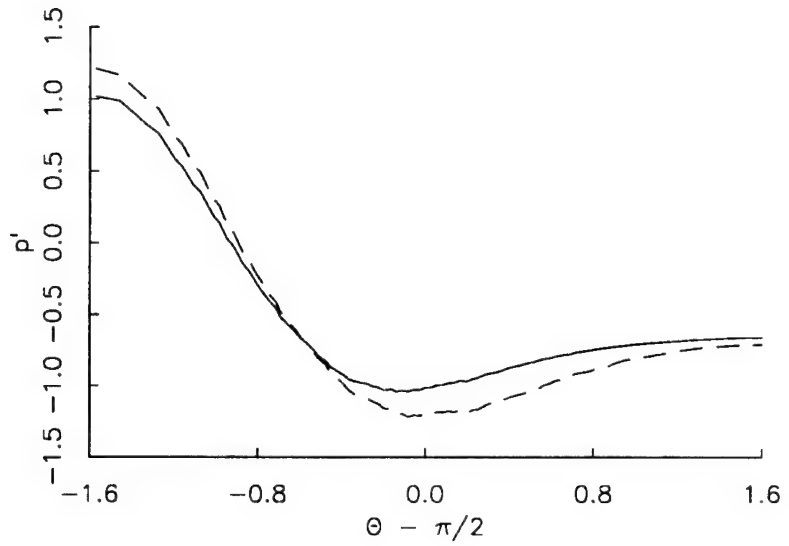

Figure 1: Dimensionless pressure $p^{'} = (p - p_{\infty})/\frac{1}{2}\rho U^2$ where p_{∞} and U are pressure and velocity far from the obstacle, as a function of $\theta - \pi/2$, where θ is the angle around the cylinder measured from the stagnation point. Laminar flow corresponds to the solid line, turbulent flow, with $l_{max}/D = 7$ to the dash-dotted line . Reynolds number $Re = 76.8$.

replaces the integral scale is the maximum length l_{max} over which exchanges can take place. (These are truncated Lévy walks.) The comparison with experiment is qualitative, because the experiments we are aware of are done at very high Reynolds number, often approaching the region of the so- called drag crisis. Our simulations are done at a Reynolds number of about 100. The quantities we will be discussing are pressure around the cylinder and drag. The question is what changes relative to the laminar case occur in these quantities, when turbulence is present, as a function of the ratio of integral scale to cylinder diameter. We will also consider the issue of coherence of the Von Karman street, when exchanges take place over larger and larger distances, transporting momentum into and out of the wake, and thus interfering with the coherent structure of the vortices. Let us discuss these items in succession:

4.1. ***Pressure around the cylinder.***

Since on the hexagonal lattice, the cross- section of the cylinder is a polygon, and not a circle, the pressure around the cylinder is measured a few units away from it, in order to minimize this effect. A comparison of laminar pressure and turbulent pressure is shown in figure 1. for our model . The ordinate is the reduced pressure $p^{'}$, and the abscissa is proportional to the angle θ around the cylinder measured from the stagnation point. Over part of the forward region

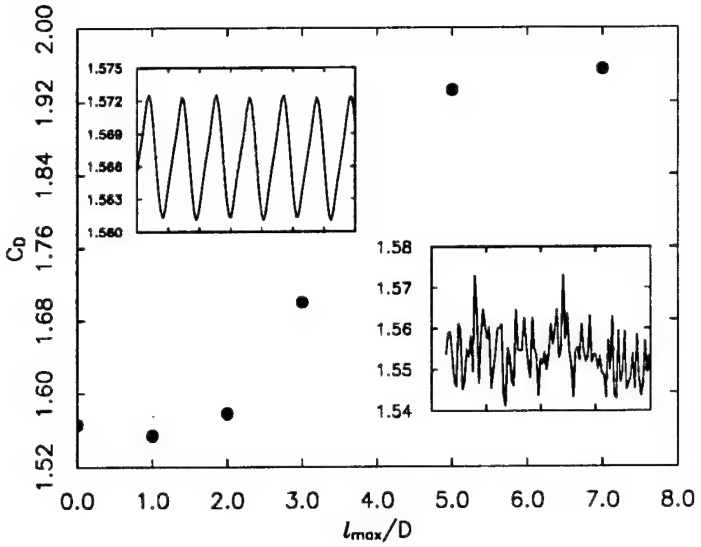

Figure 2: Drag coefficient C_D as a function of l_{max}/D. The inserts show the time series of drag in laminar flow at Re=77, and for flow with incident turbulence at $l_{max} = D$. Whereas the laminar time series is very regular, the second insert shows that even weak turbulence is strong enough to mask the small amplitude oscillations the drag undergoes as vortices are shed.

the turbulent pressure is higher than the laminar one, but around the back region the opposite is true, the greatest difference occuring close to , but above $\theta = \pi/2$. We also find (as expected) that the difference between laminar and turbulent pressure diminishes as the "integral scale" parameter l_{max}/D diminishes. These results are in qualitative agreement with those of Bearman[8] for flat plates, who observed that turbulence diminishes the base pressure (behind the plate), and also that, as the size of the plate increases (for a given integral scale) the difference between turbulent and laminar base pressure diminishes.

4.2. *Drag.*

Drag on the cylinder is affected by transport of momentum into and out of the wake, which is a result of the Lévy exhanges. These exchanges lead to a clear decrease in the size of the region of negative streamwise velocity component right behind the cylinder. From a particle point of view, this means that there are fewer particles which impinge onto the cylinder hitting it from the back against the principal thrust of the flow. As a result, the drag is expected to increase as l_{max}/D increases sufficiently. This is what is observed in figure 2 which shows the drag coefficient C_D as a function of l_{max}/D. As sooon as l_{max}/D exceeds a value of 2, the drag starts increasing. It saturates when the size of the exchanges becomes large enough to be insensitive to the dimension of the vortex

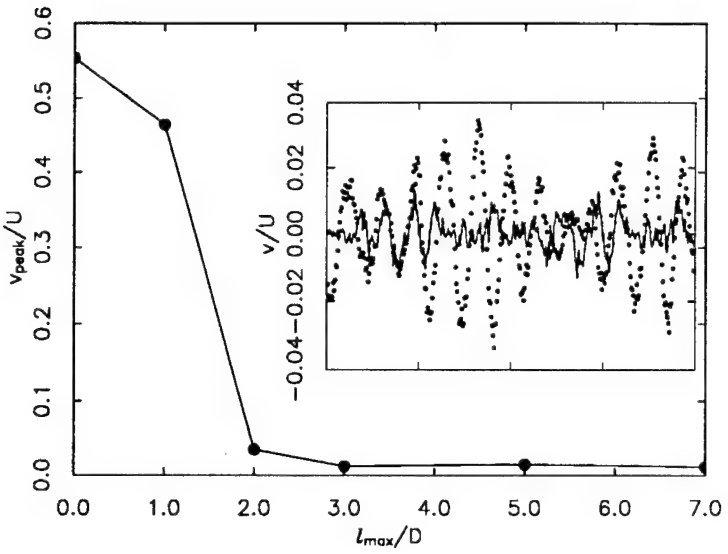

Figure 3: Transverse velocity ratio v_{peak}/U on the cylinder axis as a function of l_{max}/D. The time series for v/U is shown in the insert for $l_{max}/D = 2$(dots) and $l_{max}/D = 3$(full line). U is the average incoming velocity far from the cylinder.

street itself. According to a wake entrainment argument[8], turbulent drag should increase as $(l_{max}/D)^2$ relative to the laminar case, until it saturates. Our result on turbulent drag is in qualitative agreement with this.

4.3. *Coherence of Von Karman street.*

It is natural to ask to what extent entrainment into and out of the wake, caused by the presence of turbulence in the incident flow, affects the coherence of the Von Karman street. As a measure of that coherence, we choose the component v of velocity perpendicular to the streamwise direction, on the axis of the cylinder. In the laminar case, this is a strong component, which at the Reynolds number we are considering varies periodically in time with a well defined frequency, which determines the value of the Strouhal number. Our results illustrated in figures 3. and 4. show two things: one that v_{peak},the maximum value of v, decreases rapidly as the parameter l_{max}/D increases, and becomes very small at $l_{max}/D = 3$, the value where also the drag starts deviating significantly from the laminar value (cf. figure 2.). Secondly, that though the intensity diminishes considerably, the frequency spectrum of v continues to be dominated by the Strouhal frequency component (because of lack of statistics our power spectrum data are not of good quality.) There thus may be no significant broadening of the Strouhal peak in the spectrum as the range of exchanges increases. We have noticed however that a contour plot of pressure, which in the laminar case shows clearly the presence of vortices, changes completely as l_{max}/D becomes

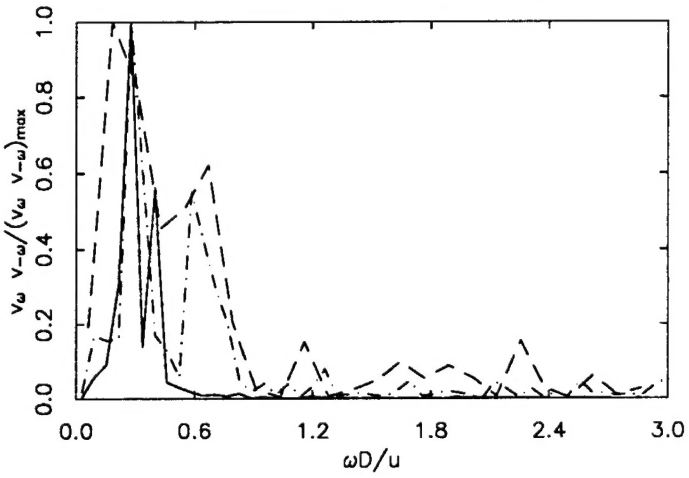

Figure 4: Power spectrum of v at a distance of $3.5D$ behind the cylinder on the cylinder axis for $l_{max} = 2D$ (solid line), $= 5D$ (dashed line), and $= 7D$ (dotted line), as a function of the dimensionless quantity (the Strouhal number) $\omega D/U$. All curves have been rescaled by their maximum value.

large enough, without any trace left of vortex structure. Correlations between transverse velocity components on and off the axis show the same phenomenon[9]. Speaking loosely, one might say that as the range of exchanges increases the Von Karman street gradually loses its spatial coherence, but in such a way that the rate of production of vortices (the Strouhal number) remains well defined, at least up to $l_{max}/D = 2$. For clearly higher values the vortices cease to exist.

There is a caveat here: these results depend sensitively on the precise relationship between $N(l)$ and l, whereas those on pressure for instance do not. It is therefore worth repeating here that as far as the coherence of the Von Karman street is concerned, our model studies only indicate what could happen and what are the parameters to measure. As to experiment, we do not know of a systematic investigation of the robustness of the Von Karman street with the integral scale of turbulence. There are indications that its robustness is not affected by turbulence[10], though an experiment on turbulent shear flow past a cylinder seems to show that vortex shedding can be disrupted at large integral scales of turbulence[11].

Acknowledgements: We are very grateful to Stephane Zaleski for his interest in this work and for helpful discussions.

This work was supported by the Department of the Navy, Office of Naval Research, under Grant No. N00014-92-J-1271, and benefitted from computer time provided by The Ohio Supercomputer Center.

References

[1] U. Frisch, B. Hasslacher, and Y. Pomeau, Phys. Rev. Lett. **56**, 1505 (1986)

[2] M. F. Shlesinger, B. J. West, and J. Klafter,Phys. Rev. Lett. **58**, 1100 (1987)

[3] L. F. Richardson, Proc. Roy. Soc. London ,Series A **110**, 709 (1926)

[4] U. Frisch, D. d'Humieres, B. Hasslacher, P. Lallemand, Y. Pomeau, and J.P. Rivet, Complex Syst. **1**, 648 (1987)

[5] P. Résibois and M. De Leener, *Classical Kinetic Theory of Fluids*, John Wiley & Sons (1977)

[6] H. Chen, S. Chen, and W. H. Matthaeus, Phys. Rev. A **45**, R5339 (1992)

[7] Lukas Wagner, Phys. Rev. E **49**, 2115 (1994); Lukas Wagner, Phys. of Fluids A, to be published

[8] P. W. Bearman, J. Fluid Mech. **46**, 177 (1971)

[9] Lukas Wagner and F. Hayot, J. of Stat. Phys., to be published.

[10] D. Surry, J. Fluid Mech. **52**, 543 (1972)

[11] M. Kiya and H. Tamura, J. of Fluids Eng. **111**, 126 (1989)

OFFICE OF THE UNDER SECRETARY OF DEFENSE (ACQUISITION)
DEFENSE TECHNICAL INFORMATION CENTER
CAMERON STATION
ALEXANDRIA, VIRGINIA 22304-6145

IN REPLY REFER TO DTIC-OCC

SUBJECT: Distribution Statements on Technical Documents

TO: OFFICE OF NAVAL RESEARCH
CORPORATE PROGRAMS DIVISION
ONR 353
800 NORTH QUINCY STREET
ARLINGTON, VA 22217-5660

1995 1027 054

1. Reference: DoD Directive 5230.24, Distribution Statements on Technical Documents, 18 Mar 87.

2. The Defense Technical Information Center received the enclosed report (referenced below) which is not marked in accordance with the above reference.

REPORT
N00014-92-J-1271
TITLE: LEVY WALKS AND TURBULENT
FLOWS

3. We request the appropriate distribution statement be assigned and the report returned to DTIC within 5 working days.

4. Approved distribution statements are listed on the reverse of this letter. If you have any questions regarding these statements, call DTIC's Cataloging Branch, (703) 274-6837.

FOR THE ADMINISTRATOR:

1 Encl

GOPALAKRISHNAN NAIR
Chief, Cataloging Branch

FL-171
Jul 93

DISTRIBUTION STATEMENT A:

APPROVED FOR PUBLIC RELEASE: DISTRIBUTION IS UNLIMITED

DISTRIBUTION STATEMENT B:

DISTRIBUTION AUTHORIZED TO U.S. GOVERNMENT AGENCIES ONLY; (Indicate Reason and Date Below). OTHER REQUESTS FOR THIS DOCUMENT SHALL BE REFERRED TO (Indicate Controlling DoD Office Below).

DISTRIBUTION STATEMENT C:

DISTRIBUTION AUTHORIZED TO U.S. GOVERNMENT AGENCIES AND THEIR CONTRACTORS; (Indicate Reason and Date Below). OTHER REQUESTS FOR THIS DOCUMENT SHALL BE REFERRED TO (Indicate Controlling DoD Office Below).

DISTRIBUTION STATEMENT D:

DISTRIBUTION AUTHORIZED TO DOD AND U.S. DOD CONTRACTORS ONLY; (Indicate Reason and Date Below). OTHER REQUESTS SHALL BE REFERRED TO (Indicate Controlling DoD Office Below).

DISTRIBUTION STATEMENT E:

DISTRIBUTION AUTHORIZED TO DOD COMPONENTS ONLY; (Indicate Reason and Date Below). OTHER REQUESTS SHALL BE REFERRED TO (Indicate Controlling DoD Office Below).

DISTRIBUTION STATEMENT F:

FURTHER DISSEMINATION ONLY AS DIRECTED BY (Indicate Controlling DoD Office and Date Below) or HIGHER DOD AUTHORITY.

DISTRIBUTION STATEMENT X:

DISTRIBUTION AUTHORIZED TO U.S. GOVERNMENT AGENCIES AND PRIVATE INDIVIDUALS OR ENTERPRISES ELIGIBLE TO OBTAIN EXPORT-CONTROLLED TECHNICAL DATA IN ACCORDANCE WITH DOD DIRECTIVE 5230.25, WITHHOLDING OF UNCLASSIFIED TECHNICAL DATA FROM PUBLIC DISCLOSURE, 6 Nov 1984 (Indicate date of determination). CONTROLLING DOD OFFICE IS (Indicate Controlling DoD Office).

The cited documents has been reviewed by competent authority and the following distribution statement is hereby authorized.

A
(Statement)

OFFICE OF NAVAL RESEARCH
CORPORATE PROGRAMS DIVISION
ONR 353
800 NORTH QUINCY STREET
ARLINGTON, VA 22217-5660

(Controlling DoD Office Name)

(Reason)

(Controlling DoD Office Address, City, State, Zip)

DEBRA T. HUGHES
DEPUTY DIRECTOR
CORPORATE PROGRAMS OFFICE
(Signature & Typed Name) (Assigning Office)

25 SEP 1996
(Date Statement Assigned)